Available online at www.sciencedirect.com
ScienceDirect
Journal of Sound and Vibration 310 (2008) 663–675
JOURNAL OF SOUND AND VIBRATION
www.elsevier.com/locate/jsvi

Frictional vibration transmission from a laterally moving surface to a traveling beam

M.R. Brake, J.A. Wickert*

Department of Mechanical Engineering and Data Storage Systems Center, Carnegie Mellon University, Pittsburgh, PA 15213, USA

Accepted 14 April 2007
The peer review of this article was organised by the Guest Editor
Available online 5 June 2007

Abstract

As the density of information stored in automated magnetic tape libraries continues to increase, greater requirements are placed on the precision of mechanical positioning in order to successfully read and write data bits. The location of the read/write head in the direction across the tape's width (termed the lateral direction) is actively controlled in order to maintain alignment between the head and data tracks, even in the presence of the tape's lateral vibration. However, during repositioning, vibration is undesirably transmitted from the laterally moving head structure to the axially moving tape because of frictional contact between the two adjacent surfaces. As an analog of that interaction, a model is developed here to describe frictional vibration transmission from a surface having prescribed lateral motion to a tensioned beam that travels and slides over it. For a transport speed that is high when compared to the lateral vibration velocity, Coulomb friction between the surface and the beam can be well-approximated by an equivalent form of viscous damping. The beam is divided into contiguous regions corresponding to free spans and the beam's portion that contacts the surface. A critical engagement length between the beam and the surface exists for which vibration transmission at a particular natural frequency can be substantially reduced, and for a given mode, that length depends weakly on the surface's position along the beam's span. By contouring the surface to have portions of differing radii of curvature, the extent of vibration transmission can be reduced over a broad range of frequency.

1. Introduction

Magnetic tape is a preferred medium for the long-term, reliable, and large-scale storage and retrieval of information. The volumetric storage density for magnetic tape has grown by six orders of magnitude during the past 50 years, in part because of advances in the mechanical design of the path, guides, cartridge, and servo mechatronics [1]. For the storage density to increase further, greater precision will be needed in the positioning of the read/write head's structure relative to the tape, even in the presence of high frequency tape vibration [2].

As data is written to the tape, or read from it, the head assembly is actively positioned in the cross-track (or lateral) direction over a data track that itself is only microns wide and that moves down-track (or axially) at

*Corresponding author.
E-mail address: wickert@cmu.edu (J.A. Wickert).

0022-460X/$ - see front matter © 2007 Elsevier Ltd. All rights reserved.
doi:10.1016/j.jsv.2007.04.029

several meters per second. During repositioning, the head's motion couples through frictional contact with the tape and undesirably excites its vibration. As an analog of that interaction, a model is developed in what follows to describe frictional vibration transmission from a surface having prescribed motion to a tensioned beam that travels and slides over it.

The vibration of magnetic tape is an application related to the broader problem area encompassing the mechanics of axially moving materials [3–5] and web transport systems [6,7]. Vibration models that are typically applied to represent magnetic and optical tape include traveling strings, and traveling tensioned beams and plates. For such systems, closed-form expressions for the response to arbitrary excitation and initial conditions are obtained through modal analysis or Green's function methods for continuous gyroscopic systems [8]. In the case of the prototypical traveling string model, a compact expression for the general response is also available through the Laplace transform method [9]. The discretization of such models and the influence of nonlinearity are discussed in Refs. [4,10,11].

Edge and surface guides are conventionally used to passively control the lateral position of tape as it is transported between a data cartridge and the drive's machine reel. In edge guiding, either rigid or compliant flanges contact the tape's narrow edge, apply lateral forces, and constrain vibration. The judicious design and placement of such guides along the path can significantly reduce the steady-state vibration amplitude [12,13], but this approach to guiding is known to accelerate wear of the tape's relatively fragile edge [14]. With guides having rigid flanges, but finite clearance between the flanges and the nominal position of the tape's edge, high-frequency vibration can be excited through intermittent impact and contact [15]. Such motion is particularly problematic in the motivating application because of the limited bandwidth over which the read/write head can be repositioned [16].

Surface guiding, on the other hand, avoids direct edge contact and instead distributes the lateral guiding forces over the substantially wider face of the tape in the form of friction. This approach is particularly appealing because of its efficacy at high frequencies. When the tape's axial velocity is large relative to the velocity of its lateral motion, conventional Coulomb friction can be well-approximated by an equivalent viscous damping model. In the related problem addressing the dynamics of a string that slides over a cylindrical guide, the equivalent damping coefficient depends on the cylinder's engagement length and radius of curvature, and the string's tension and speed [17]. Also with a view toward dissipation models in moving media, two viscous components were examined in Ref. [18] for a traveling tensioned beam: a "stationary" damping force proportional to the local velocity component, and a "moving" force that captures both local and convective velocity terms. Dry friction guides have been associated with the instability of moving string models at supercritical speeds [19,20], and the instability range extends to subcritical speeds [21] with axial acceleration.

In the present study, a model is developed for frictional vibration transmission from a laterally moving surface to a traveling beam. The design parameters that primarily influence the extent of vibration transmission are the transport speed, coefficient of friction between the beam and surface, the surface's radius of curvature, and the placement of the surface along the beam's length. A critical engagement length between the beam and the surface exists for which the vibration transmitted at a particular natural frequency of the beam can be substantially reduced. By contouring the surface to have portions of differing radii of curvature, the extent of vibration transmission can be reduced further, and over a wider range of frequency.

2. Vibration transmission model

In the path of Fig. 1, a tensioned beam travels between two stationary guides and over a portion of a cylinder having radius R. The surface of the cylinder displaces laterally, in the direction of the beam's width, with position $D(T) = D_0 e^{i\Omega T} + \text{c.c.}$, where Ω, D_0, and T denote the excitation's frequency, amplitude of motion, and time, and where $i = \sqrt{-1}$ and c.c. denotes the complex conjugate of preceding terms. The beam has bending stiffness EI, mass per unit of length ρ, tension P_1 prescribed at position $X = 0$, transport speed V, and lateral displacement U. The beam is conceptually divided into three regions: the two free spans $X \in [0, L_1)$ and $X \in (L_2, L]$ (denoted as the first and third regions in Fig. 1), and the intermediate region $X \in [L_1, L_2]$ which contacts the surface (denoted as the second region). Tension is constant in the first and third regions, but it increases exponentially because of distributed friction between the beam and surface [17]. With the

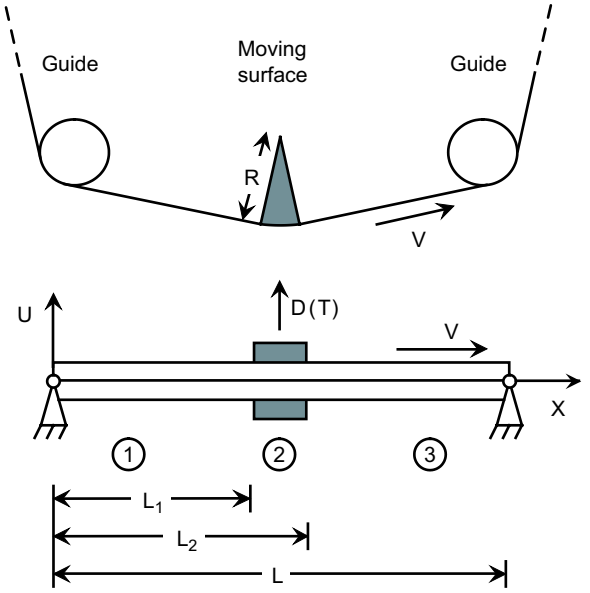

Fig. 1. Schematic of the system in which vibration is transmitted from the surface having prescribed lateral motion D to the traveling tensioned beam.

coefficient of friction denoted μ at the interface of the surface and beam, the tension profile is expressed as

$$P = \begin{cases} P_1: & 0 \leqslant X < L_1, \\ P_1 e^{\mu(X-L_1)/R}: & L_1 \leqslant X \leqslant L_2, \\ P_3 = P_1 e^{\mu(L_2-L_1)/R}: & L_2 < X \leqslant L. \end{cases} \tag{1}$$

In the second region, the normal reaction $F_N = P/R$ per unit of length develops between the surface and the beam. The frictional force acting on the beam is directed so as to oppose the velocity vector $\mathbf{V_T}$ of material particles on the beam relative to the surface. The absolute velocity of a particle on the beam has component $U_{,T} + VU_{,X}$ in the lateral direction (where the comma subscript denotes partial differentiation) and V in the axial direction. The surface's lateral velocity is simply $\dot{D}$. Under the restriction of isotropic spatial friction [22], the friction force vector per unit of length becomes

$$\mathbf{F} = -\mu F_N \frac{\mathbf{V_T}}{|\mathbf{V_T}|}, \tag{2}$$

with the lateral component

$$F_L = -\mu F_N \frac{U_{,T} + VU_{,X} - \dot{D}}{\sqrt{V^2 + (U_{,T} + VU_{,X} - \dot{D})^2}}. \tag{3}$$

In the motivating application, V is substantially greater than both $\dot{D}$ and the beam's lateral vibration velocity, and as a result, $\mathbf{F}$ rotates by only a small angle during vibration. With the approximation $\sqrt{V^2 + (U_{,T} + VU_{,X} - \dot{D})^2} \approx V$, the lateral force component over the second region becomes

$$F_L = -e^{\mu(X-L_1)/R}\left(\frac{\mu P_1}{RV}\right)(U_{,T} + VU_{,X} - \dot{D}). \tag{4}$$

In this manner, coupling between the surface and beam is equivalent to viscous damping having coefficient

$$C = e^{\mu(X-L_1)/R}\left(\frac{\mu P_1}{RV}\right) \tag{5}$$

and the lateral component of the friction force per unit of length becomes $C((U_{,T}+VU_{,X})-\dot{D})$. By defining the dimensionless quantities

$$v=V\sqrt{\frac{\rho}{P_1}},\quad v_f=\sqrt{\frac{EI}{P_1L^2}},\quad \omega=\Omega\sqrt{\frac{\rho L^2}{P_1}},\quad t=T\sqrt{\frac{P_1}{\rho L^2}},\quad c=\left(\frac{\mu P_1}{RV}\right)\frac{L}{\sqrt{P_1\rho}},$$
$$x=\frac{X}{L},\quad \ell_1=\frac{L_1}{L},\quad \ell_2=\frac{L_2}{L},\quad d=\frac{D}{L},\quad d_0=\frac{D_0}{L},\quad u=\frac{U}{L},\quad r=\frac{R}{L},\tag{6}$$

the non-dimensional equation of motion becomes [8]

$$u_{,tt}+2vu_{,xt}+\left(v^2-\frac{P}{P_1}\right)u_{,xx}-\frac{1}{P_1}\left(\frac{\mathrm{d}P}{\mathrm{d}x}\right)u_{,x}+v_f^2u_{,xxxx}$$
$$+ce^{\mu(x-\ell_1)/r}(u_{,t}+vu_{,x}-\dot{d})(H(x-\ell_1)-H(x-\ell_2))=0,\tag{7}$$

where H denotes the Heaviside function.

The solution for the beam's steady-state forced response $u^{(j)}$ in either region $j=1$ or 3 with tension P_j takes the form

$$u^{(j)}(x,t)=e^{i\omega t}\sum_{k=1}^{4}\beta_k^{(j)}e^{b_k^{(j)}x},\tag{8}$$

where the $b_k^{(j)}$ are roots of the dispersion relation

$$v_f^2(b_k^{(j)})^4+\left(v^2-\frac{P_j}{P_1}\right)(b_k^{(j)})^2+i2v\omega b_k^{(j)}-\omega^2=0.\tag{9}$$

Since the equation of motion is inhomogeneous in the second region, the solution is represented instead by the N-term power series

$$u^{(2)}(x,t)=\left(u_p^{(2)}+\sum_{k=1}^{N}\alpha_kx^{k-1}\right)e^{i\omega t},\tag{10}$$

with the particular solution

$$u_p^{(2)}=\sum_{j=0}^{M}\gamma_jx^j.\tag{11}$$

The tension profile in the second region is likewise approximated by the finite series

$$e^{\mu(x-\ell_1)/r}=\sum_{m=0}^{M}\phi_mx^m,\tag{12}$$

where

$$\phi_m=\frac{1}{m!}\sum_{k=m}^{M}\frac{(-1)^{k-m}}{(k-m)!}\left(\frac{\mu}{r}\right)^k\ell_1^{k-m}.\tag{13}$$

Substitution of Eqs. (10) and (12) into Eq. (7) yields the recurrence relation

$$(k^4+6k^3+11k^2+6k)\alpha_{k+3}+\frac{v^2}{v_f^2}(k+1)k\alpha_{k+1}+\frac{i2v\omega}{v_f^2}k\alpha_k-\frac{\omega^2}{v_f^2}\alpha_{k-1}$$
$$-\frac{1}{v_f^2}\sum_{m=0}^{M_1}((k+1-m)(k-m)\phi_m\alpha_{k+1-m})-\frac{1}{v_f^2}\sum_{m=0}^{M_2}((m+1)(k-m)\phi_{m+1}\alpha_{k-m})$$
$$+\frac{cv}{v_f^2}\sum_{m=0}^{M_1}((k-m)\phi_m\alpha_{k-m})+\frac{ic\omega}{v_f^2}\sum_{m=0}^{M_1}(\phi_m\alpha_{k-m-1})=0\tag{14}$$

for the coefficients α_k with indices $k = 1, 2, \ldots, N-4$, and

$$M_1 = \begin{cases} M: & k > M, \\ k-1: & k \leqslant M, \end{cases} \tag{15}$$

$$M_2 = \begin{cases} M-1: & k > M, \\ k-1: & k \leqslant M. \end{cases} \tag{16}$$

The coefficients γ_j in Eq. (11) are determined through a similar approach. Constants $\beta_k^{(1)}$, α_k, and $\beta_k^{(3)}$ are found through the simultaneous solution of the $N-4$ recurrence relations of Eq. (14), subject to pinned boundary conditions at $x = 0$ ($j = 1$) and at $x = 1$ ($j = 3$), and to displacement, slope, moment, and shear compatibility requirements at $x = \ell_1$ ($j = 1$) and at $x = \ell_2$ ($j = 3$), as follows:

$$\sum_{k=1}^{4} \beta_k^{(j)} \mathrm{e}^{b_k^{(j)} x} = 0, \tag{17}$$

$$\sum_{k=1}^{4} \beta_k^{(j)} (b_k^{(j)})^2 \mathrm{e}^{b_k^{(j)} x} = 0, \tag{18}$$

$$\sum_{k=1}^{4} \beta_k^{(j)} \mathrm{e}^{b_k^{(j)} x} - \sum_{k=1}^{N} \alpha_k x^{k-1} = \sum_{j=0}^{M} \gamma_j x^j, \tag{19}$$

$$\sum_{k=1}^{4} \beta_k^{(j)} b_k^{(j)} \mathrm{e}^{b_k^{(j)} x} - \sum_{k=2}^{N} \alpha_k (k-1) x^{k-2} = \sum_{j=1}^{M} \gamma_j j x^{j-1}, \tag{20}$$

$$\sum_{k=1}^{4} \beta_k^{(j)} (b_k^{(j)})^2 \mathrm{e}^{b_k^{(j)} x} - \sum_{k=3}^{N} \alpha_k (k-1)(k-2) x^{k-3} = \sum_{j=2}^{M} \gamma_j j(j-1) x^{j-2}, \tag{21}$$

$$\sum_{k=1}^{4} \beta_k^{(j)} (b_k^{(j)})^3 \mathrm{e}^{b_k^{(j)} x} - \sum_{k=4}^{N} \alpha_k (k-1)(k-2)(k-3) x^{k-4} = \sum_{j=3}^{M} \gamma_j j(j-1)(j-2) x^{j-3}. \tag{22}$$

3. Frequency response

The frequency response function describes the amplitude and phase of the beam's vibration in response to harmonic displacement D of the surface. Fig. 2 depicts the amplitude and phase responses of the beam at midspan for the illustrative parameter values $v_f = 2.83$, $v = 0.068$, $\ell_1 = 0.431$, $\ell_2 = 0.569$, and $r = 2$, which are representative of the motivating technical application. Here and in what follows, $N = 50$ and $M = 10$ in the series representations of the displacement and tension. As indicated in Table 1, those choices are sufficient to ensure accuracy in the predicted natural frequency and response amplitude. For instance, over $x \in [\ell_1, \ell_2]$, the approximation of Eq. (12) with $M = 5$ has relative error less than 10^{-8}, and the response amplitude converges to four significant digits through the fifth mode for $N \geqslant 35$. At the beam's first natural frequency ($\omega_1 = 28.0$), the relative response amplitude $|u/d_0| = 1.008$, and as the radius r is increased in Fig. 2, the magnitude at ω_1 does not change appreciably. At the third ($\omega_3 = 251$) and fifth ($\omega_5 = 698$) natural frequencies, the response amplitudes become $|u/d_0| = 1.067$ and 1.182, respectively. Resonances of the even modes are not evident in Fig. 2 because the surface is located at midspan, and speed v is small compared to the critical speed $v_c = 8.94$.

Away from resonances of the odd modes, the response's amplitude decreases with r owing to a corresponding decrease in the equivalent damping coefficient c. For instance, with a four-fold increase in r, the transmission of vibration from the surface to the beam decreases by a factor of approximately 4.5. At the anti-resonances between adjacent odd modes in Fig. 2, the phase of the response relative to the surface's motion

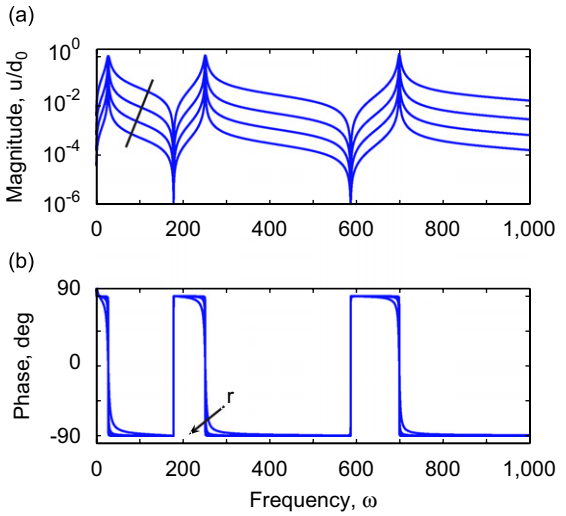

Fig. 2. (a) Magnitude and (b) phase of the beam's frequency response at $x = 0.5$ for harmonic motion of the surface; $v_f = 2.83$, $v = 0.068$, $\ell_1 = 0.431$, $\ell_2 = 0.569$, and $r = 1/32$, $1/8$, $1/2$, and 2. The arrows indicate increasing values of r.

Table 1
Convergence of the solution method as the number N of terms in the displacement's series is varied

N	Mode 1		Mode 3		Mode 5	
	ω_1	$\lvert u/d_0\rvert$	ω_3	$\lvert u/d_0\rvert$	ω_5	$\lvert u/d_0\rvert$
10	27.98	0.9847	259.6	0.01023	732.1	0.001414
15	28.01	1.008	273.2	0.1056	659.6	0.004627
20	28.01	1.008	251.3	0.9899	691.4	0.06552
25	28.01	1.008	251.4	1.067	734.2	0.9070
30	28.01	1.008	251.4	1.067	698.0	0.7841
35	28.01	1.008	251.4	1.067	698.0	1.182
40	28.01	1.008	251.4	1.067	698.0	1.182
100	28.01	1.008	251.4	1.067	698.0	1.182

For the first three odd modes, the natural frequency ω and the magnitude $|u/d_0|$ of the amplitude ratio between the beam at midspan and the surface is shown; $\ell_1 = 0.431$, $\ell_2 = 0.569$, $v_f = 2.83$, $v = 0.068$, $\mu = 0.2$, $r = 2$, and $M = 10$.

abruptly changes from -90° to 90°. Near the odd natural frequencies the phase decreases from 90° to -90° and passes through 0° at the natural frequencies. The behavior illustrated in Fig. 2, in which the amplitude $|u/d_0|$ approaches unity and the phase approaches zero at resonance, is consistent with vibration transmission through the mechanism of viscous coupling. An analog of that process is a single degree of freedom oscillator of stiffness K_s and mass M_s that is excited through the damper C_s by prescribed base displacement $D_s(T) = d_s e^{i\Omega T}$. With the mass's displacement being $U_s = u_s e^{i\Omega T}$, the complex response amplitude is

$$\frac{u_s}{d_s} = \frac{iC_s\Omega}{K_s - \Omega^2 M_s + iC_s\Omega}. \tag{23}$$

At resonance $\Omega = \sqrt{K_s/M_s}$, the amplitude is precisely that of the disturbance itself. Even as C_s grows, the amplitude at resonance remains unchanged, although the half-bandwidth of the resonant peak does increase. At resonance, the oscillator's motion is in phase with, and approximately equal in amplitude to, the disturbance.

As the transport speed is varied in Fig. 3, the even modes are not discernible in the frequency response for small v. Since the mode shapes are complex functions for $v \neq 0$, and the nodal points are not fixed in space, the even modes' contribution to the midspan response increases with v. At $\omega_2 = 112$, $|u/d_0| = 0.016$ for $v = 1$, and

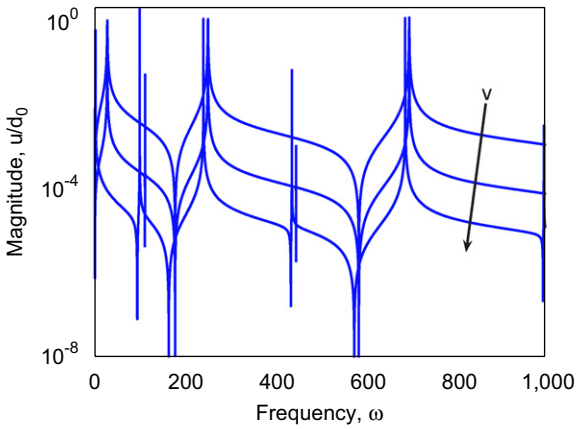

Fig. 3. Magnitude of the beam's frequency response at $x = 0.5$ as the transport speed is varied; $v_f = 2.83$, $\mu = 0.2$, $r = 2$, $\ell_1 = 0.431$, $\ell_2 = 0.569$, and $v = 0.068$, 1, and 8.9. The arrow indicates increasing values of v.

the amplitudes of the higher-frequency even modes are smaller than the amplitude of the second mode. As the speed is increased to $v = 8.9$, which is near the critical speed, the natural frequencies of all modes are lowered, the half-bandwidths of the odd modes are reduced, and the contribution of the even modes become more pronounced; for instance, $|u/d_0| = 5.3$ at ω_2.

The surface's engagement length $\ell = \ell_2 - \ell_1$, and the placement $\overline{\ell} = (\ell_2 + \ell_1)/2$ of the surface along the beam's length, can be chosen in order to minimize the level of vibration in a particular mode that is transmitted from the surface to the beam. The influence of engagement length on vibration transmission is shown in Fig. 4 at $v = 4.5$. Contours for the magnitude of the beam's midspan response are shown in Fig. 4(a) as functions of ℓ and ω. The peaks in Figs. 4(b) and (c) at $\omega = 28$, 251, and 698 correspond to the first, third, and fifth modes, respectively, and the even resonances are located at $\omega_2 = 111$ and $\omega_4 = 445$. Critical values of ℓ exist for which the response of certain modes can be significantly reduced. For instance, in Fig. 4(b), transmission to the third mode is minimized at the design point $\ell = 0.678$, and transmission to the fifth mode is minimized at $\ell = 0.402$ in Fig. 4(c).

Table 2 depicts the magnitude of steady-state response in the vicinity of ω_5, as well as the beam's corresponding displacement profiles, for three choices of the engagement length. At $\ell = 0.3$, the half-wavelength of the beam's profile extends over 67% of the surface with an antinode located at $\overline{\ell}$. Also at that condition, the beam's midspan vibrates in phase with the surface's motion. When the engagement length is alternatively chosen to equal the wavelength of the fifth mode ($\ell = 0.4$), the surface engages equal beam portions that vibrate in-phase and out-of-phase relative to the surface. At that design point, $|u/d_0|$ is reduced near ω_5 by 99.8% relative to the design $\ell = 0.3$. As the engagement length is increased further to $\ell = 0.5$ in Table 2, 60% of the surface extends over portions of the beam that move in the opposite direction of the antinode at midspan. The surface moves out-of-phase with the beam's response at midspan, but in-phase with motions at the antinodes located on either side of midspan. A second critical engagement length develops at $\ell \approx 0.8$, approximately twice the wavelength of the fifth mode, as shown in Fig. 4(a). In that case, the surface extends over equal-length portions of the beam that vibrate in-phase and out-of-phase with the surface, and $|u/d_0|$ is reduced by some 99.9% near ω_5.

The critical engagement lengths ℓ_c where transmitted vibration is minimized are identified in Fig. 5 for the third through sixth modes. At $v = 0$, the ℓ_c are integer multiples of the modal wavelengths. As v increases, ℓ_c increases by only 9% in the third mode, by 4% in the fourth mode, and by even lesser amounts in the higher modes. For the fifth and sixth modes, multiple ℓ_c exist because the wavelengths of those modes are less than half of the beam's length. The response's sensitivity to placement of the surface is shown in Fig. 6 for the fifth mode's first critical engagement length $\ell_c = 0.4$. For each $\overline{\ell}$ shown, vibration transmission to the fifth mode is reduced by nearly 99% relative to the amplitude realized in the baseline case of Fig. 2. For $\overline{\ell} < 0.5$, the even modes contribute significantly since $\overline{\ell}$ does not coincide with a nodal point of the lower even modes.

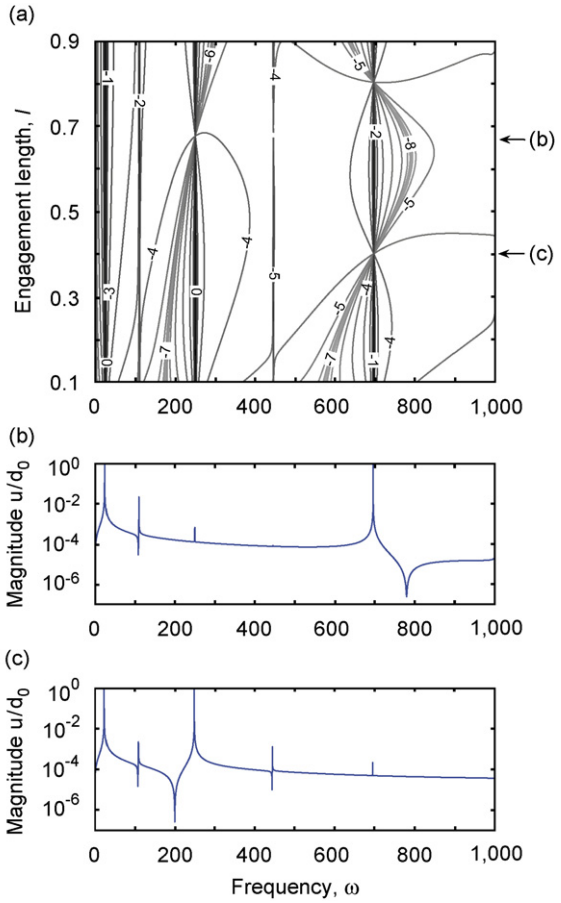

Fig. 4. (a) Magnitude of the beam's frequency response at $x = \overline{\ell} = 0.5$ as a function of the engagement length ℓ, and the frequency response magnitudes at midspan for designs (b) $\ell = 0.677$ and (c) $\ell = 0.402$; $v_f = 2.83$, $\mu = 0.2$, $r = 2$, and $v = 4.5$. Contours in (a) indicate values of $\log_{10}|u/d_0|$.

4. Optimizing surface geometry

The level of vibration that is transmitted to a particular mode can be minimized by judicious selection of the engagement length, but in that approach, the critical values of ℓ_c vary for each mode. With a view toward reducing transmission simultaneously in multiple modes, the surface can be designed as in Fig. 7 with a contour that comprises a multiplicity of regions each potentially having different radius of curvature (R_2, R_3, and R_4), engagement length, and damping coefficient (C_2, C_3, and C_4).[1] The beam's steady-state forced vibration is obtained through the procedure outlined in Eqs. (7)–(22), with the exception that five regions now comprise the two free spans $j = 1$ and 5 and the three surface regions $j = 2$, 3, and 4.

In the motivating data storage application, the beam can move bidirectionally over the surface, and in the light of that symmetry, the lengths of regions $j = 2$ and 4 and their radii of curvature are chosen to be the same; thus, $\ell_2 - \ell_1 = \ell_4 - \ell_3$, and $r_2 = r_4$. The total engagement length $\ell_T = \ell_4 - \ell_1$, the surface's inner width $\ell_i = \ell_3 - \ell_2$, and the ratio r_2/r_3 of radii are taken as the degrees of freedom in an optimization analysis in order to minimize the amplitude of response over $50 < \omega < 850$, a range that encompasses the second through fifth natural frequencies. By using a three-dimensional Nelder-Mead simplex method [23], the design

[1]The non-dimensional r_2, r_3, r_4, ℓ_3, ℓ_4, c_2, c_3, and c_4 are calculated in the same manner as r, ℓ_1, and c in Eq. (6).

Table 2
Magnitude of the beam's frequency response at $x = \overline{\ell} = 0.5$, and displacement profiles along the beam's length, for designs $\ell = 0.3$, 0.4, and 0.5; $v_f = 2.83$, $v = 0.068$, $\mu = 0.2$, and $r = 2$

ℓ	Magnitude, u/d_0	Displacement, u/d_0
0.3	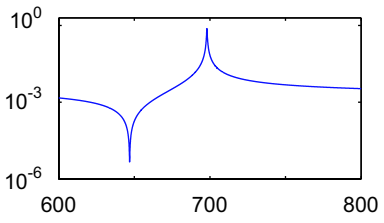	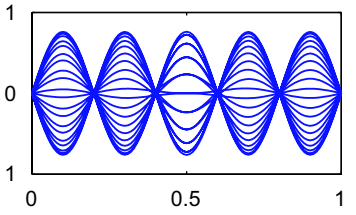
0.4	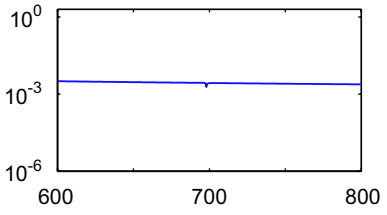	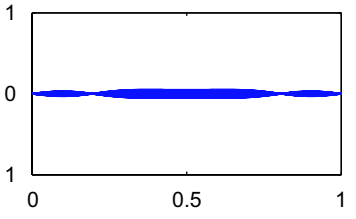
0.5	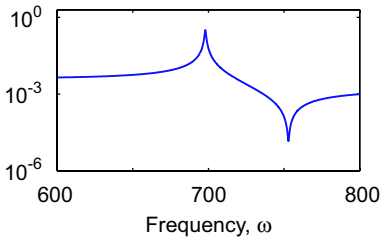	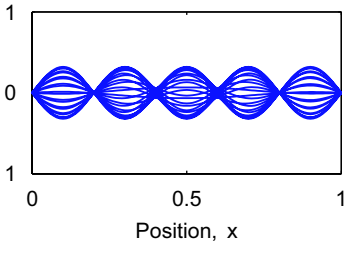

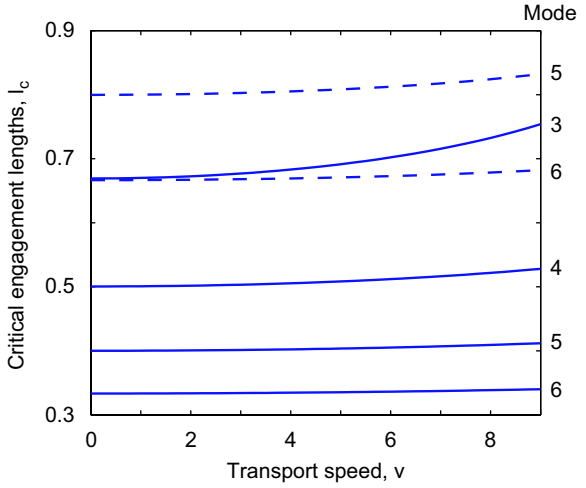

Fig. 5. First-order (——) and second-order (- - - -) critical engagement lengths between the surface and the beam for the lower vibration modes. Here $v_f = 2.83$, $\mu = 0.2$, $r = 2$, and $\overline{\ell} = 0.5$ for the third and fifth modes; $\overline{\ell} = 0.375$ for the fourth mode; and $\overline{\ell} = 0.417$ for the sixth mode.

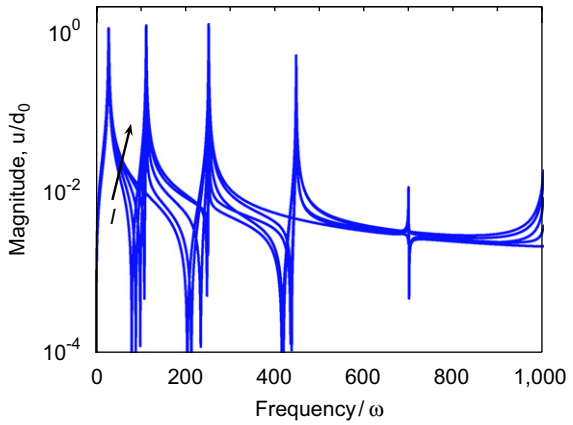

Fig. 6. Magnitude of the beam's frequency response at $x = \bar{\ell}$; $v_f = 2.83$, $v = 0.068$, $\mu = 0.2$, $r = 2$, $\ell = 0.4$, and $\bar{\ell} = 0.3$, 0.35, 0.4, 0.45, and 0.5. The arrow indicates increasing values of $\bar{\ell}$.

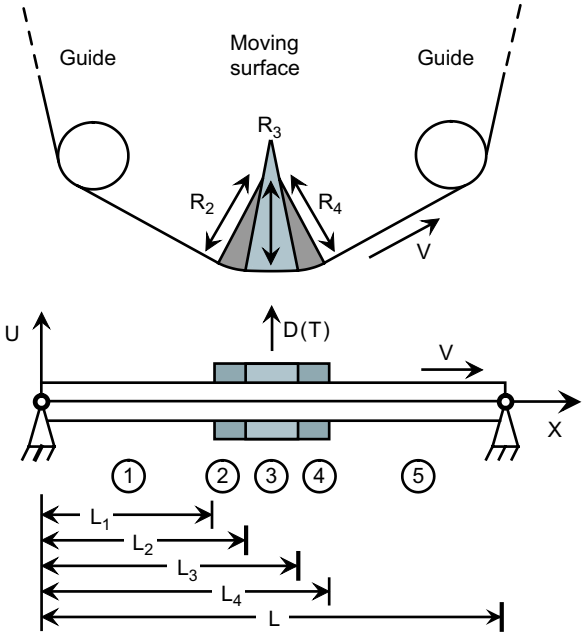

Fig. 7. Schematic of the system in which vibration is transmitted from the surface with prescribed lateral motion to the traveling tensioned beam over the second through fourth regions.

parameters are optimized in terms of the cost function

$$f_C = \sum_{n=1}^{N_S} \frac{|u_n/d_0|}{N_S}, \tag{24}$$

where u_n is the magnitude of the beam's midspan displacement at $\omega = 50 + 800(n-1)/(N_S - 1)$, and $N_S = 3001$. For the case $r_3 = 2$, the sensitivities of the optimal engagement length and radii to the transport speed are shown in Fig. 8. In optimization, the inner engagement length was driven to its bound $\ell_i = 0.01$,

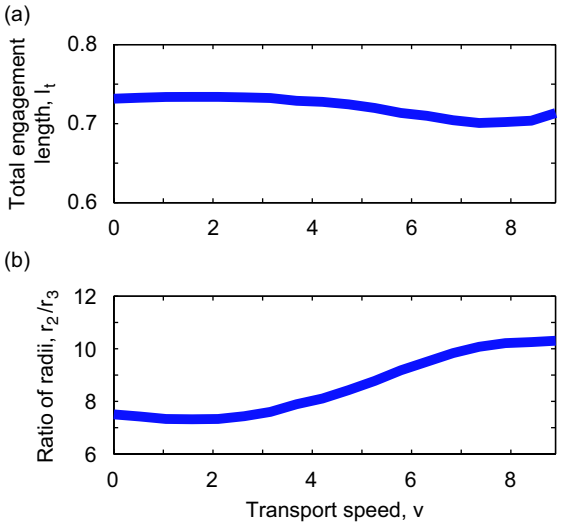

Fig. 8. Optimal (a) total engagement length and (b) ratio of radii for the surface design of Fig. 7; $r_3 = 2$ and $v_f = 2.83$. The third design parameter, the inner width, was driven to the realistic lower bound $\ell_i = 0.01$ in optimization.

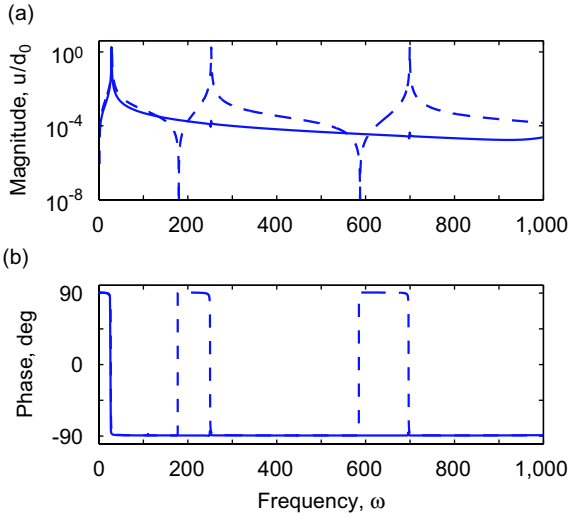

Fig. 9. (a) Magnitude and (b) phase of the beam's frequency response at $x = 0.5$ for the optimized surface (——; $\ell_T = 0.732$, $\ell_i = 0.01$, $r_2/r_3 = 7.507$, and $r_3 = 2$) comprising three regions of varying radii of curvature, and the baseline one-region surface (– – –; $\ell = 0.138$, and $r = 2$); $v_f = 2.83$, $v = 0.068$, and $\mu = 0.2$.

which is the smallest realistic value. The optimal total engagement length and radius ratio are only weakly dependent on r_3 and for a given v, they differ by less than 2% as r_3 is varied from $1/32$ to 2.

The frequency response at midspan for the optimized surface is compared in Fig. 9 to that realized with the baseline geometry with $r = r_3 = 2$. For the optimized surface, the response magnitudes at the ω_3 and ω_5 resonances have been reduced by over 99%, and the phase of the response is approximately constant over the range $50 < \omega < 1000$. While the results of the optimization are relatively insensitive to the choice of scaling parameter r_3, the response magnitude does depend on r_3 as depicted in Fig. 10. Away from resonance, as r_3 is increased by a factor of four, the magnitude of the response likewise decreases by approximately fourfold.

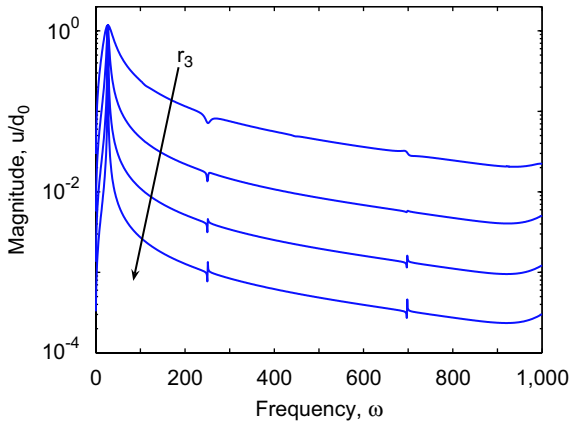

Fig. 10. Magnitude of the beam's frequency response at $x = 0.5$ for the optimized surface comprising three regions of varying radii of curvature; $v_f = 2.83$, $v = 0.068$, $\ell_T = 0.732$, $\ell_i = 0.01$, $\mu = 0.2$, $r_2/r_3 = 7.507$, and $r_3 = 1/32$, $1/8$, $1/2$, and 2. The arrow indicates increasing values of r_3.

5. Summary

A model for vibration transmission from a laterally oscillating surface to a traveling tensioned beam is developed as an analog of the interaction between a moving read/write head and magnetic tape in data storage. The level of vibration transmission can be minimized in particular vibration modes by designing the width, placement, coefficient of friction, and curvature of the surface, the contact pressure between the surface and the moving beam, and the beam's translation speed. A surface having a multiplicity of contact regions, each potentially of different length and radius of curvature, can be useful in reducing transmission to several modes simultaneously. The primary contributions and conclusions of this investigation are:

1. For a surface having a constant radius of curvature, vibration transmission from the surface to the beam can be minimized in a vibration mode by choosing an engagement length that is approximately an integer multiple of the mode's wavelength. In certain applications where it may not be feasible to implement surfaces of such width for the lower vibration modes, this approach may be useful to limit excitation of higher-frequency modes which can be more problematic in the present application.
2. A surface having a multiplicity of contact regions can be useful to reduce vibration transmission over a range of frequencies and for a chosen set of vibration modes.
3. For a surface having three contact regions as in Section 4, the optimal widths of the regions, and the ratio of the radii of curvature of the outer regions to the inner region, depend weakly on the center section's radius of curvature. However, by decreasing the radius of curvature of the center section, vibration transmission can be significantly reduced.

Acknowledgements

The authors gratefully acknowledge the support of the Information Storage Industry Consortium, and the ideas developed during technical discussions with Paul Poorman and Vern Knowles of Hewlett-Packard.

References

[1] E.R. Childers, W. Imaino, J.H. Eaton, G.A. Jaquette, P.V. Koeppe, D.J. Hellman, Six orders of magnitude in linear tape technology: the one-terabyte project, *IBM Journal of Research and Development* 47 (2003) 471–482.
[2] R.H. Dee, Magnetic tape: the challenge of reaching hard-disk-drive data densities on flexible media, *MRS Bulletin* 31 (2006) 404–408.
[3] J.A. Wickert, C.D. Mote Jr., Current research on the vibration and stability of axially-moving materials, *Shock and Vibration Digest* 20 (1988) 3–13.

[4] L.-Q. Chen, Analysis and control of transverse vibrations of axially moving strings, *ASME Applied Mechanics Reviews* 58 (2005) 91–116.
[5] C.C. Lin, Stability and vibration characteristics of axially moving plates, *International Journal of Solids and Structures* 34 (1997) 3179–3190.
[6] G.E. Young, K.N. Reid, Lateral and longitudinal dynamic behavior and control of moving webs, *ASME Journal of Dynamic Systems, Measurement, and Control* 115 (1993) 309–317.
[7] J.B. Yerashunas, J.A.D. Abreu-Garcia, T.T. Hartley, Control of lateral motion in moving webs, *IEEE Transactions on Control Systems Technology* 11 (2003) 684–693.
[8] J.A. Wickert, C.D. Mote Jr., Classical vibration analysis of axially moving continua, *ASME Journal of Applied Mechanics* 57 (1990) 738–744.
[9] W.T. van Horssen, S.V. Ponomareva, On the construction of an equation describing an axially moving string, *Journal of Sound and Vibration* 287 (2005) 359–366.
[10] F. Pellicano, F. Vestroni, Nonlinear dynamics and bifurcations of an axially moving beam, *ASME Journal of Vibration and Acoustics* 122 (2000) 21–30.
[11] J.A. Wickert, Nonlinear vibration of a traveling beam, *International Journal of Non-linear Mechanics* 27 (1992) 503–517.
[12] V. Kartik, J.A. Wickert, Vibration and guiding of moving media with edge weave imperfections, *Journal of Sound and Vibration* 291 (2006) 419–436.
[13] G. Chakraborty, A.K. Mallik, Non-linear vibration of a travelling beam having an intermediate guide, *Nonlinear Dynamics* 20 (1999) 247–265.
[14] A.V. Goldade, B. Bhushan, Tape edge study in a linear tape drive with single-flanged guides, *Journal of Magnetism and Magnetic Materials* 271 (2004) 409–430.
[15] J.M. Boyle, B. Bhushan, Vibration modeling of magnetic tape with vibro-impact of tape-guide contact, *Journal of Sound and Vibration* 289 (2006) 632–655.
[16] D.B. Richards, M.P. Sharrock, Key issues in the design of magnetic tapes for linear systems of high track density, *IEEE Transactions on Magnetics* 34 (1998) 1878–1882.
[17] K. Ono, Lateral motion of an axially moving string over a cylindrical guide surface, *ASME Journal of Applied Mechanics* 46 (1979) 905–912.
[18] D. Afolabi, Stability of a translating beam with fixed and moving viscous damping, *Journal of Sound and Vibration* 199 (1997) 701–703.
[19] S.-P. Cheng, N.C. Perkins, The vibration and stability of a friction-guided, translating string, *Journal of Sound and Vibration* 144 (1991) 281–292.
[20] J.-S. Chen, Natural frequencies and stability of an axially-traveling string in contact with a stationary load system, *ASME Journal of Vibration and Acoustics* 119 (1997) 152–157.
[21] G. Zen, S. Müftü, Stability of an axially accelerating string subjected to frictional guiding forces, *Journal of Sound and Vibration* 289 (2006) 551–576.
[22] C. Glocker, Formulation of spatial contact situations in rigid multibody systems, *Computer Methods in Applied Mechanics and Engineering* 177 (1999) 199–214.
[23] J.C. Lagarias, J.A. Reeds, M.H. Wright, P.E. Wright, Convergence properties of the Nelder-Mead simplex method in low dimensions, *SIAM Journal on Optimization* 9 (1998) 112–147.